Elastic micro-strain energy of austenite–martensite interface in NiTi

S Stupkiewicz, G Maciejewski and H Petryk

Institute of Fundamental Technological Research (IPPT PAN)
Pawińskiego 5B, 02–106 Warsaw, Poland

Abstract. The interfacial energy due to elastic micro-strains at the austenite–twinned martensite interface is calculated for the NiTi shape memory alloy undergoing cubic-to-monoclinic B2↔B19' transformation. For each crystallographically distinct microstructure, an energetically favourable local shape of the interface is determined. The approach employs finite element computations and energy minimization with respect to shape parameters, taking into account elastic anisotropy of the phases and finite-strain kinematics. The effect of atomic-scale interfacial energy is studied.
Keywords: microstructure; martensitic phase transformation; shape memory alloys (SMA); micromechanical modelling; energy minimization

PACS numbers: 68.35.Md, 81.30.Kf, 68.35.Rh, 02.70.Dh

Submitted to: *Modelling and Simulation in Materials Science and Engineering*

1. Introduction

Martensitic transformation in shape memory alloys (SMA) proceeds by formation and evolution of martensitic microstructures, and this is naturally accompanied by occurrence of interfaces at several scales. Typical examples of such interfaces are twin boundaries and austenite–martensite interfaces, and the associated interfacial energy is an important factor governing size effects [1, 2, 3, 4]. This is because the interfacial contributions to the total free energy and dissipation are *size-dependent*, i.e., they depend on characteristic dimensions of the microstructure. In effect, the actual characteristic dimensions (for instance, twin spacing and martensite plate thickness) result from the interplay of the size-dependent energy contributions at different scales. Also, the size effects on the macroscopic stress-strain response may be significant, particularly, in fine-grained materials [3, 4]. The corresponding effects can be modelled using the approaches based on minimization of the total free energy [1, 5, 6, 7, 2], or the total incremental energy including dissipation [3, 8].

There are two main sources of the interfacial energy in martensitic microstructures, namely the atomic-scale energy (e.g., the twin boundary energy) and the energy of elastic micro-strains at microstructured interfaces. An interface between austenite and

twinned martensite is a typical example of a microstructured interface where the *local* incompatibility of transformation strains is accommodated by elastic micro-strains in a thin transition layer along the interface (macroscopic compatibility of transformation strains can be satisfied by twinning). The associated interfacial energy of elastic micro-strains is, in fact, a bulk energy at a suitably fine scale, and it is interpreted as an interfacial energy at a higher scale. For a fixed morphology of the transition layer, this energy is proportional to the twin spacing, and is thus fully characterized by the corresponding *size-independent* proportionality factor [1, 9, 10].

The point is that neither the elastic micro-strain energy nor the size-independent energy factor can be measured directly. Thus, theoretical predictions or identification by inverse analysis of the associated size effects seems to be the only alternative—in both cases micromechanical modelling is indispensable. In particular, the elastic micro-strain energy factor can be predicted using the micromechanical framework developed recently in [10, 11]. Motivated by observations of corrugated interfaces between austenite and twinned martensite, cf. [12, 13, 14], this framework is based on minimization of the elastic strain energy with respect to shape parameters defining the morphology of the transition layer, i.e., the shape of the interface at the micro-scale. Within this framework, direct finite element (FE) simulations are carried out for a class of interface shapes, and energy minimization yields low-energy morphologies of the transition layer as well as the corresponding interfacial energies. The computations in [10, 11] are limited to the CuAlNi alloy undergoing the cubic-to-orthorhombic $\beta_1 \leftrightarrow \gamma_1'$ transformation. A similar analysis has recently been reported in [15] with reference to the twinned-to-detwinned interface in γ_1' martensite in CuAlNi.

The aim of this paper is to extend the methodology of calculation of the interfacial energy associated with elastic micro-strains to the NiTi shape memory alloy—the material of currently highest importance in practical applications of SMA. For that purpose, the micromechanical framework is further developed by employing the extended finite element method (X-FEM) [16] combined with the level set method [17, 18], so that discretization and analysis of arbitrary morphologies, including the saw-tooth morphology considered in this work, is easier and more accurate than in [11]. Further, the elastic anisotropy of the NiTi phases is reliably taken into account in the present computations. This is possible because the elastic constants of the monoclinic B19' martensite are now available from recent *ab initio* computations [19, 20]. Finally, application to the cubic-to-monoclinic transformation (as in NiTi) requires that the full non-symmetric transformation gradient is used as eigen-distorsion rather than only the symmetric transformation stretch as, e.g., in the case of the cubic-to-orthorhombic transformation in CuAlNi.

As a result of the present analysis, energetically favourable shapes of the local interface between austenite and martensite are calculated along with the respective interfacial energy factors for all crystallographically distinct microstructures at the austenite–martensite interface in NiTi. The nominal (i.e., macroscopic) interface is the habit plane of orientation predicted by the crystallographic theory of martensite

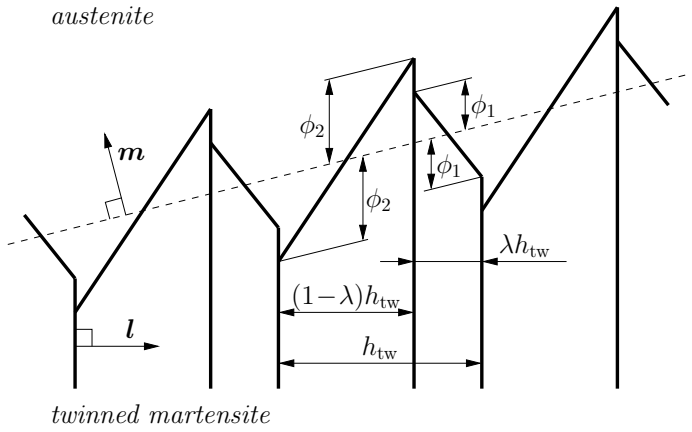

Figure 1. Sketch of saw-tooth morphology of the transition layer at the austenite–twinned martensite interface.

[21, 22, 23], while the local interface shape exhibits significant fluctuations around the nominal plane. Such results are obtained for the first time for NiTi.

Similarly as in the vast majority of micromechanical models of NiTi, only the B2 austenite and B19' martensite are considered. The possibility of formation of the intermediate R-phase is not examined in view of its relatively small transformation strain. Moreover, the R-phase is usually absent during the reverse B19'→B2 transformation.

2. Micromechanical framework

The micromechanical framework employed in this work is briefly presented in this section, while more details can be found in [10, 11]. However, we do provide here the extensions and details specifically related to the present application of the framework to the NiTi SMA.

The analysis is concerned with the transition layer at the austenite–twinned martensite interfaces. The microstructure at the interface (which is macroscopically compatible at zero stress) is determined using the crystallographic theory of martensite [21, 22, 23]. In particular, three geometrical parameters are computed for each microstructure: the twinning plane unit normal $\boldsymbol{l}$, the unit vector $\boldsymbol{m}$ normal to the *macroscopic* austenite–martensite interface (habit plane), and the twin fraction λ, cf. Fig. 1.

Previous calculations for CuAlNi [11] have indicated that a simple two-parameter saw-tooth morphology of the interface layer can be used to predict both the interfacial energy and the low-energy morphologies, as the corresponding results are reasonably close to those obtained for a much richer shape parameterization involving 18 shape parameters. In the present work, we exploit this result and only consider the saw-tooth morphologies. A periodic saw-tooth morphology and the corresponding two shape parameters ϕ_1 and ϕ_2 are shown in Fig. 1. A zigzag-shaped interface is obtained for

$\phi_1 = \phi_2$, while $\phi_1 = \phi_2 = 0$ corresponds to a planar interface.

The adopted saw-tooth interface morphology is rather simple and cannot represent more complex geometrical features that might possibly accompany formation of austenite–twinned martensite interfaces. For instance, bending of martensite domains has been observed and modelled at the single variant–twinned martensite interfaces [24, 25], while experimental evidence of similar effects at the austenite–twinned martensite interfaces is missing. A possible effect of bending of twin interfaces was included in the previous energy calculations done for CuAlNi alloy in [11] but was found to be not substantial.

The present approach does not include sequential twin branching [6, 26, 27]. However, since the elastic micro-strain energy is concentrated here in vicinity of the austenite-martensite interface, the obtained results can still be applied to estimate the interfacial energy at the finest scale of branching twins reaching the austenite boundary.

The FE analysis is carried out for a two-dimensional periodic unit cell constructed in the plane that contains the normal vectors $\boldsymbol{l}$ and $\boldsymbol{m}$. However, the stresses and strains correspond to the fully three-dimensional case.

The finite-strain framework is adopted, and multiplicative decomposition of the deformation gradient $\boldsymbol{F}$ is assumed,

$$\boldsymbol{F} = \boldsymbol{F}^{\mathrm{e}}\boldsymbol{F}^{\mathrm{t}}, \tag{1}$$

where $\boldsymbol{F}^{\mathrm{e}}$ and $\boldsymbol{F}^{\mathrm{t}}$ denote the elastic and the transformation part, respectively ($\boldsymbol{F}^{\mathrm{t}} = \boldsymbol{1}$ for austenite). The simple St. Venant–Kirchhoff model of anisotropic hyperelasticity with eigenstrains is adopted so that the elastic strain energy

$$W_{\mathrm{e}} = \frac{1}{2}(\det \boldsymbol{F}^{\mathrm{t}})\boldsymbol{E}^{\mathrm{e}}\boldsymbol{L}\boldsymbol{E}^{\mathrm{e}} \tag{2}$$

is quadratic in the elastic Green strain tensor $\boldsymbol{E}^{\mathrm{e}} = \frac{1}{2}(\boldsymbol{F}^{\mathrm{eT}}\boldsymbol{F}^{\mathrm{e}} - \boldsymbol{1})$, as in [10, 28]. Here, $\boldsymbol{L}$ denotes the elastic moduli tensor determined in the intermediate configuration, and W_{e} refers to a unit reference volume of unstressed austenite. We have checked that the use of the logarithmic strain measure in Eq. (2) instead of the Green strain $\boldsymbol{E}^{\mathrm{e}}$ only slightly affects the present results (the difference in energy factor $\Gamma^{\mathrm{e}}_{\mathrm{am}}$ is typically about 1%).

Distinct elastic anisotropy of NiTi phases is incorporated by using the elastic constants of the cubic austenite found from ultrasonic measurements [29] and of the monoclinic B19' martensite available from recent *ab initio* computations [19], see also [20]. Special attention must be paid to specify correctly the transformation part $\boldsymbol{F}^{\mathrm{t}}$ of the deformation gradient and the elastic moduli tensor $\boldsymbol{L}$ of the martensite variants. The elastic constants of B19' computed in [19] define the components $L_{i'j'k'l'}$ of $\boldsymbol{L}$ in a local Cartesian coordinate system such that its basis vectors $\boldsymbol{e}'_1$ and $\boldsymbol{e}'_2$ are co-linear with the lattice vectors, $\boldsymbol{a} = a\boldsymbol{e}'_1$ and $\boldsymbol{b} = b\boldsymbol{e}'_2$, while $\boldsymbol{e}'_3 = \boldsymbol{e}'_1 \times \boldsymbol{e}'_2$ is *not* aligned with the lattice vector $\boldsymbol{c} = c(\cos\beta\boldsymbol{e}'_1 + \sin\beta\boldsymbol{e}'_3)$ due to the monoclinic angle $\beta \neq 90°$. The components of the (nonsymmetric) deformation gradient $\boldsymbol{F}^{\mathrm{t}}$ in this local coordinate

system are

$$F^{\mathrm{t}}_{i'j'} = \begin{pmatrix} \hat{\alpha} & 0 & \hat{\gamma}\cos\beta \\ 0 & \hat{\beta} & 0 \\ 0 & 0 & \hat{\gamma}\sin\beta \end{pmatrix}, \tag{3}$$

where $\hat{\alpha} = a/\sqrt{2}a_0$, $\hat{\beta} = b/\sqrt{2}a_0$, $\hat{\gamma} = c/a_0$, and a_0 is the lattice constant of the austenite. Both $L_{i'j'k'l'}$ and $F^{\mathrm{t}}_{i'j'}$ must be transformed to the global coordinate system associated with the cubic basis of the austenite. Adopting the lattice correspondence such that $\boldsymbol{e}'_1 = \frac{1}{\sqrt{2}}(1,1,0)$, $\boldsymbol{e}'_2 = \frac{1}{\sqrt{2}}(-1,1,0)$ and $\boldsymbol{e}'_3 = (0,0,1)$ in this global coordinate system, the corresponding components of $\boldsymbol{F}^{\mathrm{t}}$ are given by

$$F^{\mathrm{t}}_{ij} = R_{ii'}R_{jj'}F^{\mathrm{t}}_{i'j'}, \qquad R_{ii'} = \begin{pmatrix} \frac{1}{\sqrt{2}} & -\frac{1}{\sqrt{2}} & 0 \\ \frac{1}{\sqrt{2}} & \frac{1}{\sqrt{2}} & 0 \\ 0 & 0 & 1 \end{pmatrix}, \tag{4}$$

and similarly $L_{ijkl} = R_{ii'}R_{jj'}R_{kk'}R_{ll'}L_{i'j'k'l'}$, where $R_{ii'}$ is the rotation matrix. The above lattice correspondence happens to define martensite variant 9, according to the numbering of variants used in [23]. Indeed, the (symmetric) transformation stretch tensor $\boldsymbol{U}^{\mathrm{t}}$, such that $(\boldsymbol{U}^{\mathrm{t}})^2 = (\boldsymbol{F}^{\mathrm{t}})^{\mathrm{T}}\boldsymbol{F}^{\mathrm{t}}$ with $\boldsymbol{F}^{\mathrm{t}}$ determined according to Eqs. (3)–(4), coincides with the transformation stretch tensor of variant 9 (cf. [23], page 55),

$$(\boldsymbol{U}^{\mathrm{t}}_9)_{ij} = \begin{pmatrix} \alpha & \delta & \epsilon \\ \delta & \alpha & \epsilon \\ \epsilon & \epsilon & \gamma \end{pmatrix}, \tag{5}$$

where α, γ, δ and ϵ are the transformation stretch parameters. Clearly, the consistent transformation parts of the deformation gradient and elastic moduli tensors of the remaining variants are obtained by appropriate rotation of, respectively, $\boldsymbol{F}^{\mathrm{t}}$ and $\boldsymbol{L}$ defined above for variant 9.

In this work, the extended FE method known as X-FEM [16] is used to solve the boundary value problem on a mesh that is not conforming to the interfaces (phase boundaries). This is an improvement with respect to the approach used in [11] in the case of the saw-tooth morphology, where the spatial distribution of the phases was approximated at the level of Gauss points. The X-FEM is combined with the level set method [17], and two level sets are used in order to effectively specify the location of the three phases (austenite and two twin-related crystallographic variants of martensite) and of the three types of interfaces [18]. The X-FEM enrichment strategy proposed in [30] has been used in combination with eight-node serendipity displacement-based elements and bilinear interpolation of level sets. The enrichment function is discontinuous in its derivative across the interface and vanishes on the elements that are not crossed by interfaces. The enriched elements are triangulated and integration is performed independently for each material domain.

For a fixed morphology of the transition layer, i.e., for given shape parameters ϕ_1 and ϕ_2, the elasticity problem at zero macroscopic stress is solved directly. Adopting the geometric parameters (λ, $\boldsymbol{l}$, $\boldsymbol{m}$) from the crystallographic theory guarantees that the

twinned martensite is *macroscopically* compatible with the austenite, so that the elastic strains decay quickly with the distance from the interface, and far-field stresses are zero. Subsequently, the total elastic strain energy $\overline{W}_{\mathrm{e}}$ within the unit cell is computed, and the interfacial energy of elastic micro-strains $\gamma^{\mathrm{e}}_{\mathrm{am}}$ is determined by referring $\overline{W}_{\mathrm{e}}$ to the nominal area A_{macro} of the macroscopic austenite–martensite interface within the unit cell. From the dimensional analysis it follows that the elastic micro-strain energy $\gamma^{\mathrm{e}}_{\mathrm{am}}$ is proportional to twin spacing h_{tw}. Hence, an energy factor $\Gamma^{\mathrm{e}}_{\mathrm{am}}$ is introduced [10],

$$\Gamma^{\mathrm{e}}_{\mathrm{am}} = \frac{\gamma^{\mathrm{e}}_{\mathrm{am}}}{h_{\mathrm{tw}}}, \qquad \gamma^{\mathrm{e}}_{\mathrm{am}} = \frac{\overline{W}_{\mathrm{e}}}{A_{\mathrm{macro}}}, \tag{6}$$

which depends on the morphology of the transition layer, i.e., in the present calculations, on shape parameters ϕ_1 and ϕ_2, and for a fixed morphology is *size-independent*. In practical terms, this also implies that finite element computations of $\Gamma^{\mathrm{e}}_{\mathrm{am}}$ can be carried out for an arbitrary twin spacing.

As the final step, the elastic micro-strain energy factor $\Gamma^{\mathrm{e}}_{\mathrm{am}}$ is minimized with respect to shape parameters ϕ_1 and ϕ_2. This minimization reflects the assumed ability of the transforming material to adjust its microstructure (here, the shape of the interface) so that the free energy is as low as possible. In this work, the conjugate gradient method [31] has been used as the minimization algorithm, and the corresponding solutions have been refined using the BFGS method [31]. The required gradients of the objective function have been determined numerically by the finite difference method.

The atomic-scale energy of local austenite-martensite interfaces is expected to penalize deviation from planar interface, as the corresponding contribution to the total free energy is proportional to the total area of the interface at the micro-scale. To account for this effect, the total interfacial energy γ_{am} has been considered,

$$\gamma_{\mathrm{am}} = \psi\gamma^{\mathrm{a}}_{\mathrm{am}} + \Gamma^{\mathrm{e}}_{\mathrm{am}} h_{\mathrm{tw}}, \qquad \psi = \frac{A_{\mathrm{micro}}}{A_{\mathrm{macro}}} \geq 1, \tag{7}$$

where $\gamma^{\mathrm{a}}_{\mathrm{am}}$ denotes the atomic-scale energy per unit area of the interface, in the lack of respective data assumed here as a constant (independent of the orientation, etc.), and ψ is the ratio of the total area A_{micro} of the austenite–martensite interfaces at the micro-scale to the macroscopic area A_{macro}. The purely geometrical factor ψ is the lowest for a planar interface ($\psi = 1$). Now, the total interfacial energy γ_{am}, rather than the interfacial energy of elastic micro-strains alone, can be minimized with respect to shape parameters. Note that the shape parameters affect γ_{am} through $\Gamma^{\mathrm{e}}_{\mathrm{am}}$ and ψ, while $\gamma^{\mathrm{a}}_{\mathrm{am}}$ and h_{tw} are kept constant.

3. Results and discussion

In the cubic-to-monoclinic B2→B19' transformation in NiTi, there are 192 macroscopically compatible austenite–twinned martensite microstructures [23], of which eight crystallographically distinct microstructures can be chosen, and the remaining ones can be obtained by applying rotations from the symmetry point group of cubic austenite. Table 1 provides the geometrical parameters of the eight representative microstructures

Table 1. Crystallographically distinct microstructures at the austenite–twinned martensite interface in NiTi.

	Twin fraction λ	Twinning plane normal $\boldsymbol{l}$	Habit plane normal $\boldsymbol{m}$
B-I-1	0.2976	(0, 1, 0)	(0.9169, 0.3188, −0.2402)
B-I-2	0.2976	(0, 1, 0)	(0.2963, −0.4190, 0.8583)
B-II-1	0.2710	(0.6121, 0, −0.79080)	(0.8941, 0.3997, −0.2022)
B-II-2	0.2710	(0.6121, 0, −0.79080)	(0.3313, −0.5119, 0.7925)
C-I-1	0.3101	(0.7071, −0.7071, 0)	(0.8686, 0.2328, 0.4374)
C-I-2	0.3101	(0.7071, −0.7071, 0)	(0.0172, −0.8379, 0.5455)
C-II-1	0.3221	(0.2693, 0.2693, 0.9246)	(0.9201, 0.1552, 0.3596)
C-II-2	0.3221	(0.2693, 0.2693, 0.9246)	(0.05663, −0.9090, 0.4130)

Table 2. Size-independent elastic micro-strain energy factor $\Gamma^{\mathrm{e}}_{\mathrm{am}}$ [MJ/m^3].

Interface shape	B-I-1	B-I-2	B-II-1	B-II-2	C-I-1	C-I-2	C-II-1	C-II-2
planar	23.5	21.6	16.1	21.0	32.0	19.5	24.9	30.6
zigzag	20.4	11.1	13.1	18.4	30.2	9.7	16.4	24.0
saw-tooth	20.3	11.1	13.1	18.2	30.0	9.7	16.3	23.3

that have been analyzed in this work. The labeling convention is the following. The first letter denotes the twinning mode. Twinning modes B and C are represented here by the (1,3) and (1,5) variant pairs, respectively, and the twin fraction λ denotes the volume fraction of martensite variant 1 (numbering of variants as in [23]). The Roman number denotes the type of twin interface (type I or type II), and two habit plane orientations are enumerated by the last digit (1 or 2). The transformation stretch parameters ($\alpha = 1.025$, $\gamma = 0.959$, $\delta = 0.062$, $\epsilon = -0.049$) used to compute the microstructural parameters in Table 1 have been determined using the lattice constants ($a_0 = 3.015\,\text{Å}$, $a = 4.646\,\text{Å}$, $b = 4.108\,\text{Å}$, $c = 2.898\,\text{Å}$, $\beta = 97.78°$) reported by Kudoh et al. [32].

Table 2 contains the values of the size-independent energy factor $\Gamma^{\mathrm{e}}_{\mathrm{am}}$ calculated for each of the eight representative microstructures (Table 1) by minimizing the elastic micro-strain energy (i.e., the effect of the atomic-scale interfacial energy is disregarded here). As a reference, the results corresponding to planar and optimal zigzag-shaped interfaces are also included in Table 2. The values of $\Gamma^{\mathrm{e}}_{\mathrm{am}}$ corresponding to zigzag and saw-tooth interfaces are seen to be very close to each other. At the same time, the values of $\Gamma^{\mathrm{e}}_{\mathrm{am}}$ of planar interfaces are significantly higher than those obtained by shape minimization. For instance, in the case of microstructures B-I-2 and C-I-2, the elastic micro-strain energy of the saw-tooth interface of optimal shape is approximately twice lower than the energy of the planar interface. In the other cases the reduction is between 6 and 35%.

The calculated saw-tooth morphologies that minimize the elastic micro-strain energy are shown in Fig. 2. In all cases the shape of the interface is rather close

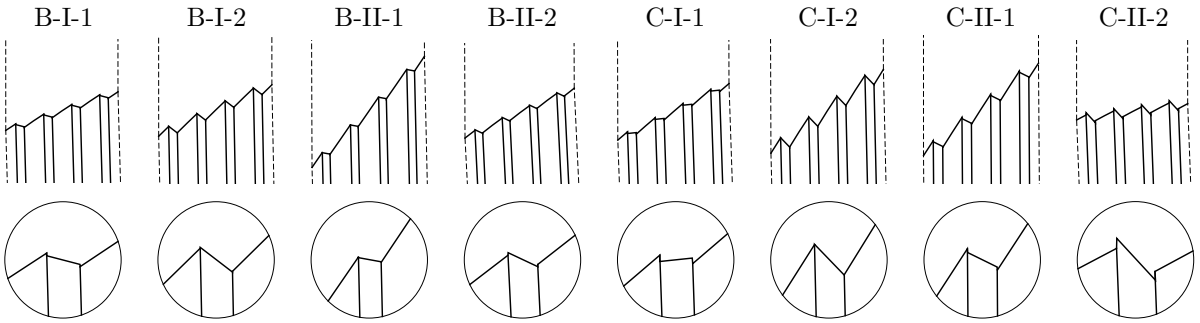

Figure 2. Calculated low-energy saw-tooth morphologies of the eight crystallographically distinct microstructures of the transition layer at the austenite–martensite interface in NiTi (obtained by minimization of the elastic micro-strain energy).

Table 3. Effect of twin spacing h_{tw} on the minimum total interfacial energy γ_{am} of C-I-2 microstructure and its elastic and atomic-scale contributions.

h_{tw} [nm]	$\Gamma^{\mathrm{e}*}_{\mathrm{am}}$ [MJ/m^3]	$\gamma^{\mathrm{e}}_{\mathrm{am}}$ [J/m^2]	$\psi\gamma^{\mathrm{a}}_{\mathrm{am}}$ [J/m^2]	γ_{am} [J/m^2]
100	9.8	0.98	0.41	1.39
20	11.2	0.22	0.35	0.58

to a zigzag shape. This is consistent with the observation that the values of $\Gamma^{\mathrm{e}}_{\mathrm{am}}$ corresponding to zigzag and saw-tooth interfaces are very close to each other.

In order to estimate the effect of atomic-scale energy $\gamma^{\mathrm{a}}_{\mathrm{am}}$ on the morphology of the austenite–martensite interface and on the associated elastic micro-strain energy, an additional study has been performed in which the *total* interfacial energy γ_{am}, cf. Eq. (7), has been minimized with respect to shape parameters ϕ_1 and ϕ_2. In this case, the morphology itself depends on the twin spacing, and so does (albeit slightly) the calculated energy factor (6), for convenience distinguished here by a star. It is emphasized that the twin spacing is prescribed in this analysis. Determination of the twin spacing itself, e.g., as a function of grain size in polycrystalline SMA, is a separate problem which requires consideration of size-dependent interfacial energy contributions at all relevant scales, cf. [33, 3].

As an example, the C-I-2 microstructure corresponding to the lowest energy factor $\Gamma^{\mathrm{e}}_{\mathrm{am}}$ in Table 2 has been considered, and representative results are presented in Table 3 and in Fig. 3. Results for two values of the twin spacing h_{tw} are displayed, $h_{\mathrm{tw}} = 20$ nm and $h_{\mathrm{tw}} = 100$ nm, which approximately correspond to the twin spacing limits predicted by a micromechanical model in [34] for subgrain size varying between 10 and 200 μm, respectively. In view of the lack of respective experimental data, a rough estimate of the atomic-scale energy has been adopted as $\gamma^{\mathrm{a}}_{\mathrm{am}} = 0.3$ J/m^2, cf. [3, 34].

As expected, the atomic-scale interfacial energy penalizes the deviation from planar interface, and the effect is more pronounced for smaller twin spacing. The associated variation of the morphology of the transition layer is accompanied by an increase of the elastic micro-strain energy factor $\Gamma^{\mathrm{e}*}_{\mathrm{am}}$ with respect to the minimum value in Table 2

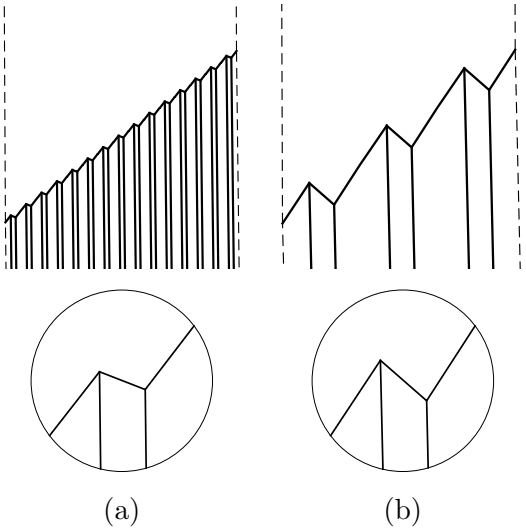

Figure 3. Effect of twin spacing $h_{\rm tw}$ on the morphologies that minimize the total interfacial energy: C-I-2 microstructure for (a) $h_{\rm tw} = 20$ nm and (b) $h_{\rm tw} = 100$ nm.

obtained by minimization of the elastic-strain energy alone (i.e., corresponding to large $h_{\rm tw}$). However, in quantitative terms the difference is not large (15% increase of $\Gamma^{\rm e*}_{\rm am}$ for a rather small twin spacing of 20 nm). The influence on morphology is also moderate, cf. Fig. 3. Note that even for a small $h_{\rm tw} = 20$ nm, a significantly non-planar interface is still obtained.

In view of the above observations, a reasonable estimate of the total interfacial energy $\gamma_{\rm am}$ is obtained by neglecting the influence of the atomic-scale interfacial energy on the morphology, i.e., by using $\Gamma^{\rm e}_{\rm am}$ and ψ that correspond to the morphology obtained by minimization of the elastic strain energy alone. The difference is negligible for $h_{\rm tw} = 100$ nm and is well below 10% for $h_{\rm tw} = 20$ nm.

4. Conclusions

The interfacial energy of elastic micro-strains at the austenite–twinned martensite interface has been estimated for NiTi shape memory alloy undergoing B2↔B19' transformation. Specifically, the size-independent energy factors have been calculated for all crystallographically distinct microstructures at the austenite–martensite interface by applying a micromechanical framework based on energy minimization. These factors can directly be used within the general energy-based theoretical framework [8] to calculate size effects in evolving martensitic microstructures, e.g., as in [3, 34].

It has been shown that a significantly lower interfacial energy is typically obtained for an optimal non-planar interface in comparison to that corresponding to a strictly planar interface. There exists some experimental evidence [12, 13, 14] that the austenite–twinned martensite interfaces are indeed non-planar at the micro-scale, as predicted by our analysis. However, detailed experimental characterization of such interfaces in SMA,

and in NiTi in particular, is still missing.

Finally, theoretical analysis, e.g., such as that carried out in this work, seems to be the only way to obtain quantitative estimates of the elastic micro-strain energy which can hardly be determined experimentally.

Acknowledgments

This work has been partially supported by the Polish Ministry of Science and Higher Education through grant no. N N501 267734.

References

[1] A. G. Khachaturyan. *Theory of Structural Transformations in Solids*. John Wiley and Sons, New York, 1983.

[2] T. Waitz, T. Antretter, F. D. Fischer, N. K. Simha, and H. P. Karnthaler. Size effects on the martensitic phase transformation of NiTi nanograins. *J. Mech. Phys. Solids*, 55:419–444, 2007.

[3] H. Petryk, S. Stupkiewicz, and G. Maciejewski. Interfacial energy and dissipation in martensitic phase transformations. Part II: Size effects in pseudoelasticity. *J. Mech. Phys. Solids*, 58:373–389, 2010.

[4] Y. Chen and C. A. Schuh. Size effects in shape memory alloy microwires. *Acta Mater.*, 59:537–553, 2011.

[5] G. R. Barsch and J. A. Krumhansl. Twin boundaries in ferroelastic media without interface dislocations. *Phys. Rev. Lett.*, 53(11):1069–1072, 1984.

[6] R. V. Kohn and S. Müller. Branching of twins near an austenite–twinned-martensite interface. *Phil. Mag. A*, 66(5):697–715, 1992.

[7] X. Ren and L. Truskinovsky. Finite scale microstructures in nonlocal elasticity. *J. Elasticity*, 59:319–355, 2000.

[8] H. Petryk and S. Stupkiewicz. Interfacial energy and dissipation in martensitic phase transformations. Part I: Theory. *J. Mech. Phys. Solids*, 58:390–408, 2010.

[9] A. L. Roytburd. Thermodynamics of polydomain heterostructures. II. Effect of microstresses. *J. Appl. Phys.*, 83(1):239–245, 1998.

[10] G. Maciejewski, S. Stupkiewicz, and H. Petryk. Elastic micro-strain energy at the austenite–twinned martensite interface. *Arch. Mech.*, 57:277–297, 2005.

[11] S. Stupkiewicz, G. Maciejewski, and H. Petryk. Low-energy morphology of the interface layer between austenite and twinned martensite. *Acta Mater.*, 55:6292–6306, 2007.

[12] K. M. Knowles and D. A. Smith. The nature of the parent–martensite interface in titanium–manganese. *Acta Metall.*, 29:1445–1466, 1981.

[13] M. J. Hÿtch, Ph. Vermaut, J. Malarria, and R. Portier. Study of atomic displacement fields in shape memory alloys by high-resolution electron microscopy. *Mater. Sci. Eng. A*, 273–275:266–270, 1999.

[14] D. Z. Liu and D. Dunne. Atomic force microscope study of the interface of twinned martensite in copper-aluminium-nickel. *Scripta Mater.*, 48(12):1611–1616, 2003.

[15] H. Seiner, O. Glatz, and M. Landa. A finite element analysis of the morphology of the twinned-to-detwinned interface observed in microstructure of the Cu–Al–Ni shape memory alloy. *Int. J. Sol. Struct.*, 48:2005–2014, 2011.

[16] T. Belytschko and T. Black. Elastic crack growth in finite elements with minimal remeshing. *Int. J. Num. Meth. Engng.*, 45:601–620, 1999.

[17] J. A. Sethian. *Level Set Methods and Fast Marching Methods: Evolving Interfaces in*

Computational Geometry, Fluid Mechanics, Computer Vision, and Materials Science. Cambridge University Press, Cambridge, UK, 2nd edition, 1999.

[18] S. Zlotnik and P. Diez. Hierarchical X-FEM for n-phase flow ($n > 2$). *Comp. Meth. Appl. Mech. Engng.*, 198:2329–2338, 2009.

[19] M. F. X. Wagner and W. Windl. Lattice stability, elastic constants and macroscopic moduli of NiTi martensites from first principles. *Acta Mater.*, 56:6232–6245, 2008.

[20] N. Hatcher, O. Yu. Kontsevoy, and A. J. Freeman. Role of elastic and shear stabilities in the martensitic transformation path of NiTi. *Phys. Rev. B*, 80:144203, 2009.

[21] M. S. Wechsler, D. S. Lieberman, and T. A. Read. On the theory of the formation of martensite. *Trans. AIME J. Metals*, 197:1503–1515, 1953.

[22] J. M. Ball and R. D. James. Fine phase mixtures as minimizers of energy. *Arch. Ration. Mech. Anal.*, 100:13–50, 1987.

[23] K. Bhattacharya. *Microstructure of martensite: why it forms and how it gives rise to the shape-memory effect*. Oxford University Press, Oxford, 2003.

[24] P. Boullay, D. Schryvers, and R. V. Kohn. Bending martensite needles in Ni65Al35 investigated by two-dimensional elasticity and high-resolution transmission electron microscopy. *Phys. Rev. B*, 64:144105, 2001.

[25] A. Finel, Y. Le Bouar, A. Gaubert, and U. Salman. Phase field methods: Microstructures, mechanical properties and complexity. *C. R. Physique*, 11:245–256, 2010.

[26] R. D. James, R. V. Kohn, and T. W. Shield. Modeling of branched needle microstructures at the edge of a martensite laminate. *J. Physique IV*, C8:253–259, 1995.

[27] S. Conti. Branched microstructures: scaling and asymptotic self-similarity. *Comm. Pure Appl. Math.*, 53:1448–1474, 2000.

[28] M. Kružik, A. Mielke, and T. Roubiček. Modelling of microstructure and its evolution in shape-memory-alloy single-crystals, in particular in CuAlNi. *Meccanica*, 40:389–418, 2005.

[29] O. Mercier, K. N. Melton, G. Gremaud, and J. Hagi. Single-crystal elastic constants of the equiatomic NiTi alloy near the martensitic tranformation. *J. Appl. Phys.*, 51:1833–1834, 1980.

[30] N. Möes, M. Cloirec, P. Cartaud, and J. F. Remacle. A computational approach to handle complex microstructure geometries. *Comp. Meth. Appl. Mech. Engng.*, 192:3163–3177, 2003.

[31] J. Nocedal and S. J. Wright. *Numerical Optimization*. Springer, New York, 2nd edition, 2006.

[32] Y. Kudoh, M. Tokonami, S. Miyazaki, and K. Otsuka. Crystal-structure of the martensite in Ti-49.2at%Ni alloy analyzed by the single-crystal X-ray-diffration method. *Acta Metall.*, 33:2049–2056, 1985.

[33] H. Petryk, S. Stupkiewicz, and G. Maciejewski. Modelling of austenite/martensite laminates with interfacial energy effect. In Q. P. Sun and P. Tong, editors, *IUTAM Symposium on Size Effects on Material and Structural Behavior at Micron- and Nano-scales, Hong-Kong 2004*, volume 142 of *Solid Mechanics and its Applications*, pages 151–162. Springer, 2006.

[34] S. Stupkiewicz and H. Petryk. Grain-size effect in micromechanical modelling of hysteresis in shape memory alloys. *ZAMM*, 90:783–795, 2010.